Supplementary Information for: Reactivity of free 1,3-diisopropyl-4,5-dimethylimidazol-2-ylidene in dichloromethane

Magnus R. Buchner*[a] and Deniz F. Bekiş[a]

Philipps-Universität Marburg

Contents

1 Experimental data

Caution! Beryllium and its compounds are categorized as human carcinogens and work with these substances is associated with severe health hazards.[1] As the biochemical mechanisms that cause beryllium associated diseases are still unknown,[2–4] special safety and administrative precautions are strongly advised.[1]

1.1 General experimental techniques

All manipulations were performed under an inert gas atmosphere of argon either by working in a glove box or by using *Schlenk* techniques. CaH_2 was used for CD_2Cl_2 and CH_2Cl_2. Subsequently the deuterated solvent was vacuum distilled before storage in an argon-filled glove box. Reactions were carried out and NMR spectra were recorded in *J. Young* NMR tubes which were silylated according to the literature procedure.[5] **^{Me}IPr**,[6] **IDipp**,[7] [(**IDipp**)$BeBr_2$],[8] and $BeBr_2$ were synthesised following literature procedures.[9] [(**^{Me}IPr**)$BeBr_2$] and [(**^{Me}IPr$_2$**)$BeBr_2$] were synthesised according to a modified published procedure,[10] where THF was used instead of C_6H_6 due to superior solubility and reaction rates.

1.2 X-ray structure determination

A crystal of [**^{Me}IPr**H]Cl was selected under a pre-dried in perfluorinated oil and mounted using the MiTeGen MicroLoop system at ambient temperature. X-ray diffraction data was collected using the monochromated Cu-$K_{\overline{\alpha}}$ ($\lambda = 1.541\,86$ Å) radiation of a *Stoe* StadiVari diffractometer equipped with a *Xenocs* Microfocus Source and a *Dectris* Pilatus 300 K detector. Evaluation, integration and reduction of the diffraction data was carried out using the X-AREA software suite.[11] Multi-scan absorption correction was applied with the LANA module of the X-AREA software suite. The structures were solved with dual-space methods (SHELXT-2018/2) and refined against F_2 (SHELXL-2018/3) using the OLEX2 software package.[12–14] All atoms were located by Difference Fourier synthesis and non-hydrogen atoms refined anisotropically. Hydrogen atoms were refined using the "riding model" approach with isotropic displacement parameters 1.2 times that of the connected carbon atom. Representations of the crystal structures were created with the Diamond software.[15] CCDC 2281578 contain the Supplementary crystallographic data for this paper. This data can be obtained free of charge from The Cambridge Crystallographic Data Centre.

1.3 NMR spectroscopy

^{1}H, ^{9}Be and ^{13}C NMR spectra were recorded on *Bruker* Avance III HD300 and Avance III AV500 spectrometers. The latter was equipped with a Prodigy Cryo-Probe. ^{1}H (300/500 MHz) and ^{13}C (76/126 ppm) NMR chemical shifts are given relative to the solvent signal for CD_2Cl_2 (5.32 and 53.8 ppm). ^{9}Be (42 MHz) NMR spectroscopy used 0.43 [M] $BeSO_4$ in D_2O as an external standard. NMR spectra were processed with the *Mestrenova* software package.[16]

1.4 IR spectroscopy

IR spectra were recorded on a *Bruker* alpha FTIR spectrometer equipped with a diamond ATR unit in an argon-filled glovebox. Processing of the spectra was performed with the OPUS[17] software package and *Mestrenova*.[16]

1.5 Raman spectroscopy

The Raman spectra were recorded on an *S&I* Confocal Raman Microscope MonoVista CRS+ at ambient temperature. The Raman spectrometer was equipped with four laser diodes with excitation lines of 488 nm, 532 nm, 633 nm and 785 nm.

1.6 Mass Spectrometry

HR-ESI mass spectra were acquired with an Orbitrap Q *Thermo Fischer Scientific* Exactive plus mass spectrometer. The resolution was set to 140000.

1.7 Synthetic procedures and characterization

1.7.1 Synthesis of [^{Me}IPrH]Cl

Inside a glovebox 9.6 mg (0.053 mmol) ^{Me}**IPr** was weighed into a *J. Young* NMR tube and 0.5 ml CH_2Cl_2 was added *via* air-displacement pipette. After 72 h the solvent was removed *in vacuo* and the red residue redissolved in CD_2Cl_2. Removal of the solvent gave the title compound in quantitative yield as a light red solid. Crystals of [^{Me}**IPr**H]Cl were obtained by suspending the red residue in C_6D_6 and heating to 80 °C for 24 h.
^{1}H NMR (300 MHz, CD_2Cl_2) δ = 1.68 (d, $^3J_{HH}$ = 6.8 Hz, 12H, CH(CH_3)$_2$), 2.23 (s, 6H, CH_3), 4.49 (p, $^3J_{HH}$ = 6.8 Hz, 2H, CH(CH$_3$)$_2$), 10.85 (s, 1H, CH). ^{13}C NMR (75 MHz, CD_2Cl_2) δ = 8.8 (*C*H$_3$), 23.1 (CH(*C*H$_3$)$_2$), 51.4 (*C*H(CH$_3$)$_2$), 125.8 ((CH$_3$)*C*=*C*(CH$_3$)), 134.8 (*C*H). FT-IR (cm^{-1}): 3098 (w), 2972 (m), 2925 (s), 2898 (m), 2780 (w), 2745 (w), 1770 (w), 1654 (m), 1630 (m), 1550 (s), 1460 (s), 1444 (s), 1395 (n), 1375 (m), 1342 (s), 1293 (w), 1242 (vs), 1195 (s), 1142 (m), 1118 (s), 1046 (w), 938 (w), 893 (m), 775 (w), 728 (w), 663 (s), 610 (w), 594 (w), 540 (m), 432 (w).

1.7.2 Reactivity of IDipp in CD_2Cl_2

Inside a glovebox 10 mg (0.026 mmol) **IDipp** was weighed into a *J. Young* NMR tube and 0.5 ml CD_2Cl_2 was added *via* air-displacement pipette. NMR spectra were recorded in regular intervals.

1.7.3 Synthesis of [(^{Me}IPr)$BeBr_2$]

Inside a glovebox 9.0 mg (0.05 mmol, 1 eq.) ^{Me}**IPr** and 8.4 mg (0.05 mmol, 1 eq.) $BeBr_2$ were weighed into a *J. Young* NMR tube and 0.5 ml CD_2Cl_2 were added *via* air-displacement pipette. NMR spectra were recorded after 2 h reaction time and are identical to those obtained from dissolving [(^{Me}**IPr**)$BeBr_2$] in CD_2Cl_2 and show quantitative conversion without noticeable side products.
^{1}H NMR (500 MHz, CD_2Cl_2) δ = 1.59 (d, $^3J_{HH}$ = 6.9 Hz, 12H, CH(CH_3)$_2$), 2.19 (s, 6 H, C=CCH_3), 4.45 (hept, $^3J_{HH}$ = 6.8 Hz, 2 H, CH(CH$_3$)$_2$. ^{9}Be NMR (42 MHz, CD_2Cl_2) δ = 13.3 ($\omega_{1/2}$ = 70.3 Hz). ^{13}C NMR (126 MHz, CD_2Cl_2) δ = 9.5 (s, C=C*C*H$_3$), 23.1 (s, CH(*C*H$_3$)$_2$), 51.6 (s, *C*H(CH$_3$)$_2$), 125.9 (s, N*C*=*C*N), 163.2 (s, N*C*N, $\omega_{1/2}$ = 71.6 Hz).

1.7.4 Synthesis of [(^{Me}IPr)$_2$$BeBr_2$]

Inside a glovebox 18.0 mg (0.10 mmol, 2 eq.) ^{Me}**IPr** and 8.4 mg (0.05,mmol, 1 eq.) $BeBr_2$ were weighed into a *J. Young* NMR tube and 0.5 ml CD_2Cl_2 were added *via* air-displacement pipette. NMR spectra were recorded after 12 h reaction time and are identical to those obtained from dissolving [(^{Me}**IPr**)$_2$$BeBr_2$] in CD_2Cl_2 and show quantitative conversion without noticeable side products.
^{1}H NMR (300 MHz, CD_2Cl_2) δ = 1.29 (d, $^3J_{HH}$ = 7.2 Hz, 24H, CH(CH_3)$_2$), 2.20 (s, 12 H, C=CCH_3), 5.79 (hept, $^3J_{HH}$ = 7.2 Hz, 2 H, CH(CH$_3$)$_2$. ^{9}Be NMR (42 MHz, CD_2Cl_2) δ = 1.9 ($\omega_{1/2}$ = 36.1 Hz). ^{13}C NMR (126 MHz, CD_2Cl_2) δ = 10.6 (s, C=C*C*H$_3$), 21.4 (s, CH(*C*H$_3$)$_2$), 51.1 (s, *C*H(CH$_3$)$_2$), 125.4 (s, N*C*=*C*N), 172.8 (s, N*C*N, $\omega_{1/2}$ = 64.6 Hz).

1.7.5 Synthesis of [(IDipp)$BeBr_2$]

Inside a glovebox 11.5 mg (0.03 mmol, 1 eq.) **IDipp** and 5.0 mg (0.03 mmol, 1 eq.) $BeBr_2$ were weighed into a *J. Young* NMR tube and 0.5 ml CD_2Cl_2 were added *via* air-displacement pipette. NMR spectra were recorded after 2 h reaction time are identical to those obtained from dissolving [(**IDipp**)$BeBr_2$] in CD_2Cl_2 and show quantitative conversion without noticeable side products.
^{1}H NMR (500 MHz, CD_2Cl_2) δ = 1.16 (d, $^3J_{HH}$ = 6.9 Hz, 12H, CH(CH_3)$_2$), 1.35 (d, $^3J_{HH}$ = 6.8 Hz, 12H, CH(CH_3)$_2$), 2.63 (hept, $^3J_{HH}$ = 6.8 Hz, 4H, CH(CH$_3$)$_2$), 7.26 (s, 2H, NCH), 7.31 – 7.39 (m, 4H, H_{Ph}), 7.50 – 7.59 (m, 2H, H_{Ph}). ^{9}Be NMR (42 MHz, CD_2Cl_2) δ = 13.6 ($\omega_{1/2}$ = 80.5 Hz). ^{13}C NMR (126 MHz, CD_2Cl_2) δ = 23.0 (s, CH(*C*H$_3$)$_2$), 25.9 s, CH(*C*H$_3$)$_2$), 29.2 (s, *C*H(CH$_3$)$_2$), 124.6 (s, C_{Ph}H), 125.0 (s, N*C*H), 131.3 (s, C_{Ph}H), 133.6 (s, C_{Ph}), 146.1 (s, C_{Ph}), 170.5 (s, N*C*N, $\omega_{1/2}$ = 61.0 Hz).

2 Crystallographic data

Table S1: Crystal data and details of the structure determination of [$^{\mathbf{Me}}$**IPr**H]Cl.

Empirical formula	$C_{11}H_{21}ClN_2$
Relative molecular mass g mol^{-1}	216.75
Crystal system	monoclinic
Space group (No.)	$P2_1/n$ (14)
Radiation / Å	1.54186
a / Å	11.5065(11)
b / Å	7.5925(5)
c / Å	15.0274(14)
β / °	104.919(8)
V / Å^3	1268.59(19)
Z	4
colour	light red
crystal morphology	block
crystal size / mm	$0.092 \times 0.067 \times 0.039$
$F(000)$ / e	472.0
$\rho_{\text{calc.}}$ / g cm^{-3}	1.135
μ / mm^{-1}	2.393
θ range / °	8.68–151.5
Range of Miller indices	$-13 \leq h \leq 14$
	$-7 \leq k \leq 9$
	$-18 \leq l \leq 13$
Reflections collected; unique	12584; 2579
Restraints; parameters	0; 156
R_{int}	0.0296
wR_1 ($I \geq 2\sigma(I)$)	0.0462
R_1 (all data)	0.0568
wR_2 ($I \geq 2\sigma(I)$)	0.1223
wR_2 (all data)	0.1274
S	1.050
$\Delta\rho_{\text{min}}$, $\Delta\rho_{\text{max}}$ / e Å^{-3}	−0.21; 0.34

3 NMR spectroscopic data

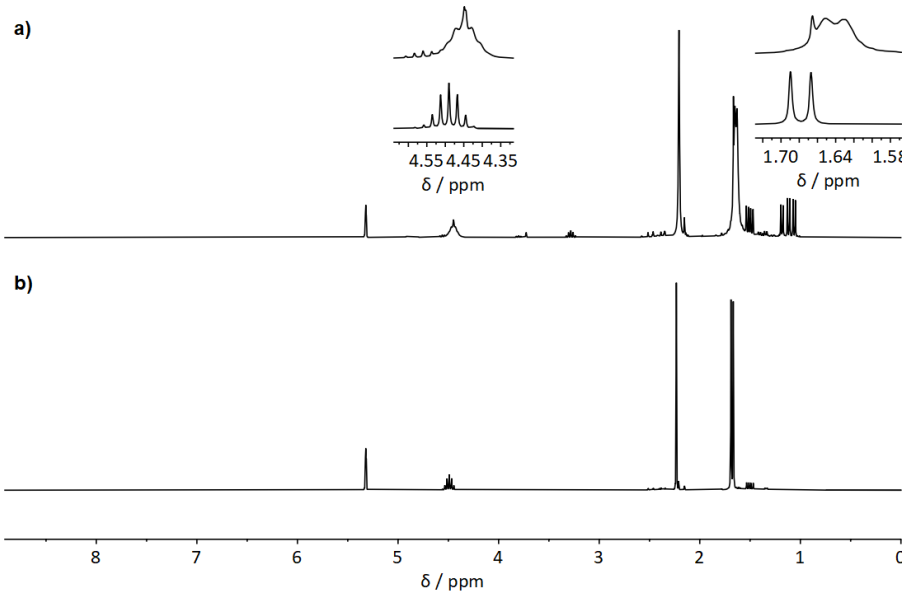

Figure S1: ^{1}H NMR spectrum of $^{\mathrm{Me}}$**IPr** in CD_2Cl_2 at T = 300 K after a) 3 h and b) 72 h.

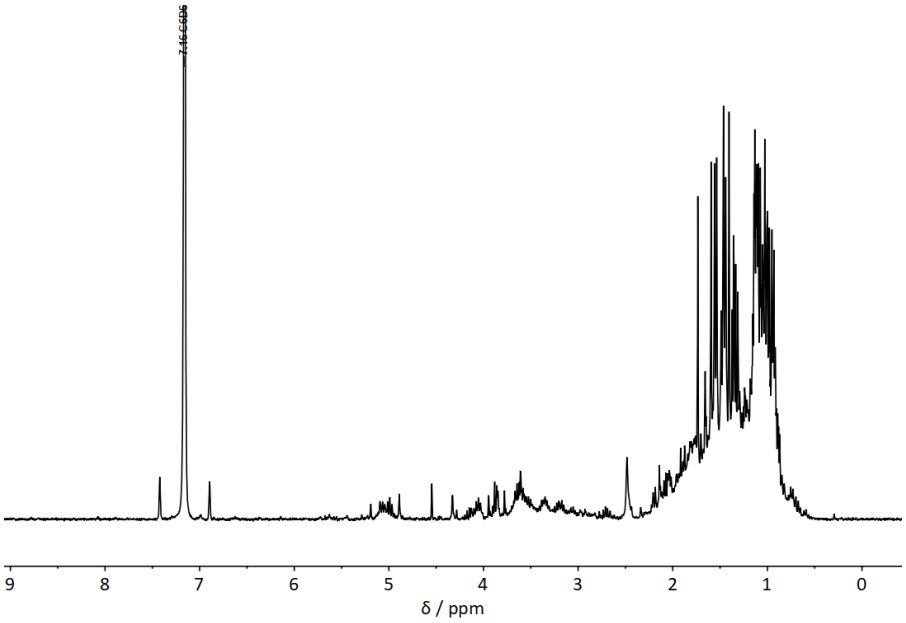

Figure S2: ^{1}H NMR spectrum in C_6D_6 (T = 300 K) of the product mixture of the reaction of $^{\mathrm{Me}}$**IPr** with CD_2Cl_2.

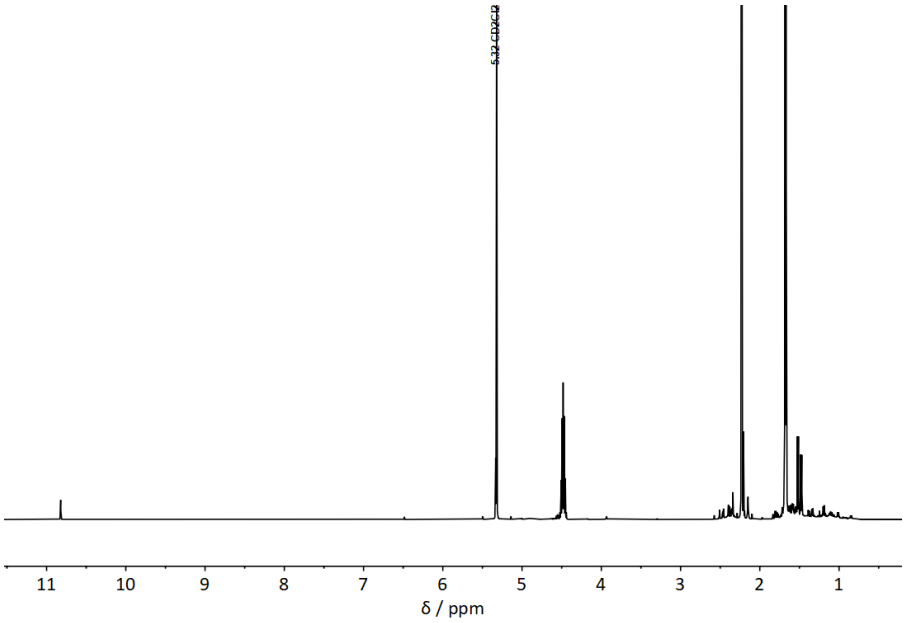

Figure S3: ^{1}H NMR spectrum of [$^{\mathbf{Me}}$**IPr**H/D]Cl in CD_2Cl_2 at T = 300 K.

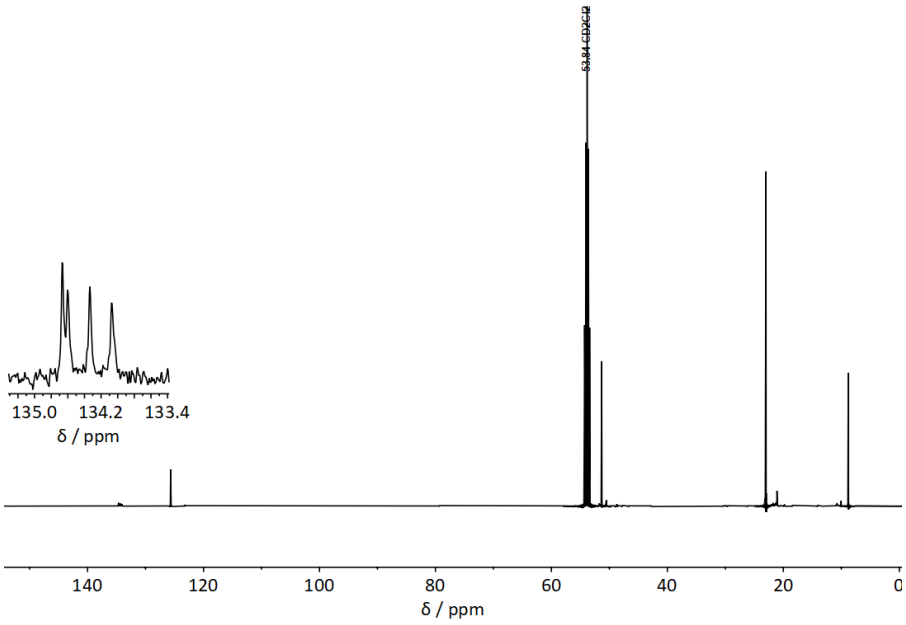

Figure S4: ^{13}C{^{1}H} NMR spectrum of [iPrH/D]Cl in CD_2Cl_2 at T = 300 K.

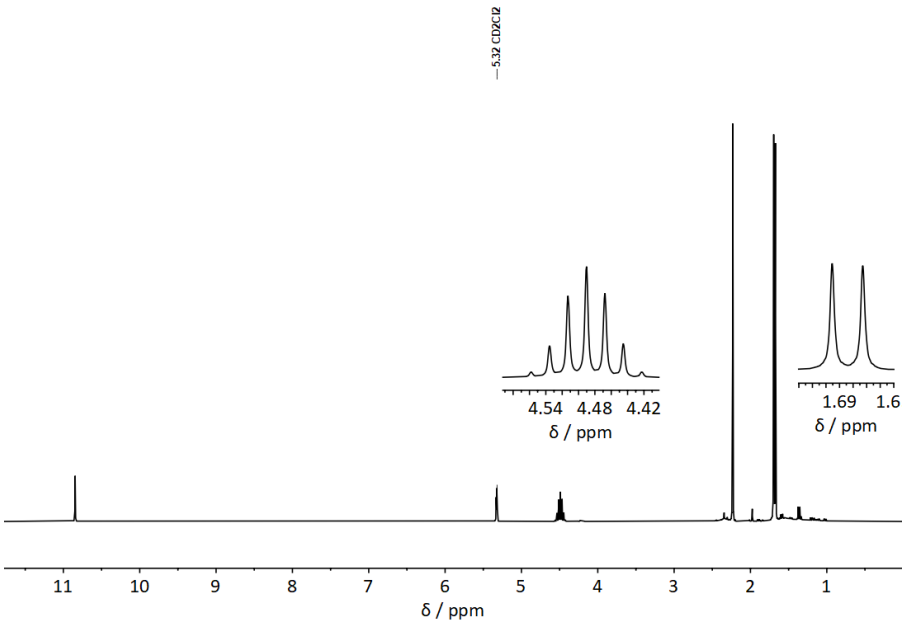

Figure S5: ^{1}H NMR spectrum of [$^{\mathbf{Me}}$**IPr**H]Cl in CD_2Cl_2 at T = 300 K.

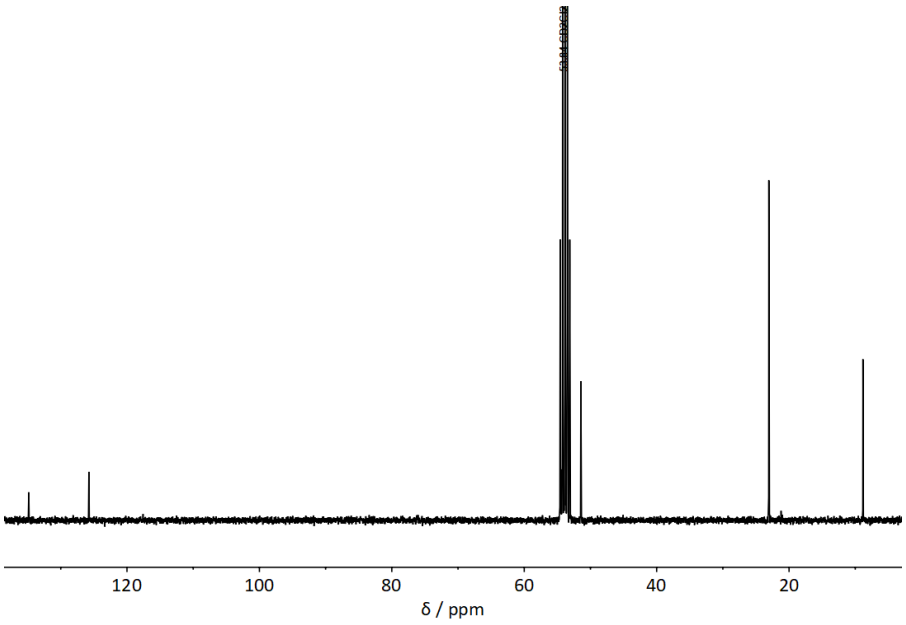

Figure S6: ^{13}C{^{1}H} NMR spectrum of [iPrH]Cl in CD_2Cl_2 at T = 300 K.

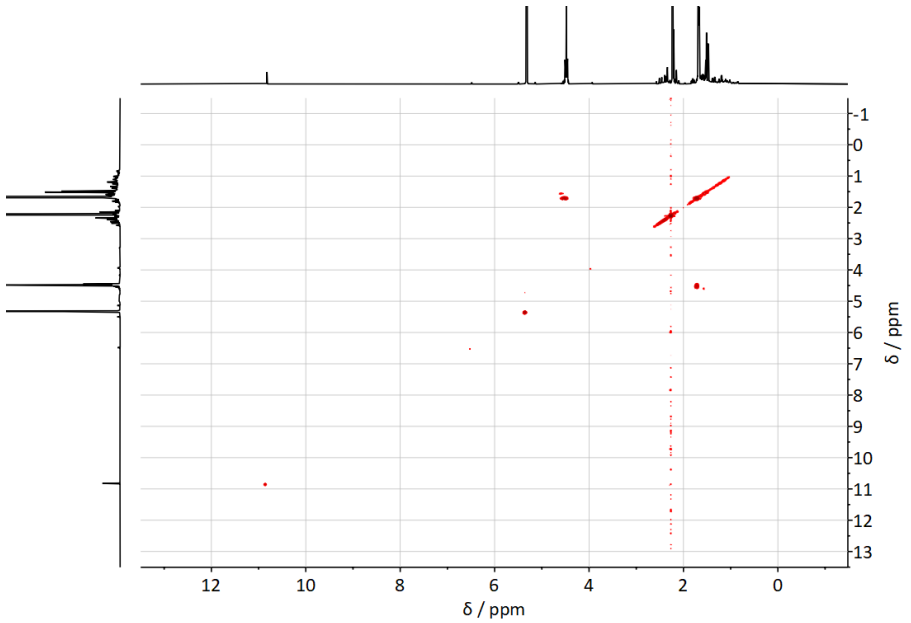

Figure S7: $^{1}H^{1}H$ COSY NMR spectrum of [iPrH/D]Cl in CD_2Cl_2 at T = 300 K.

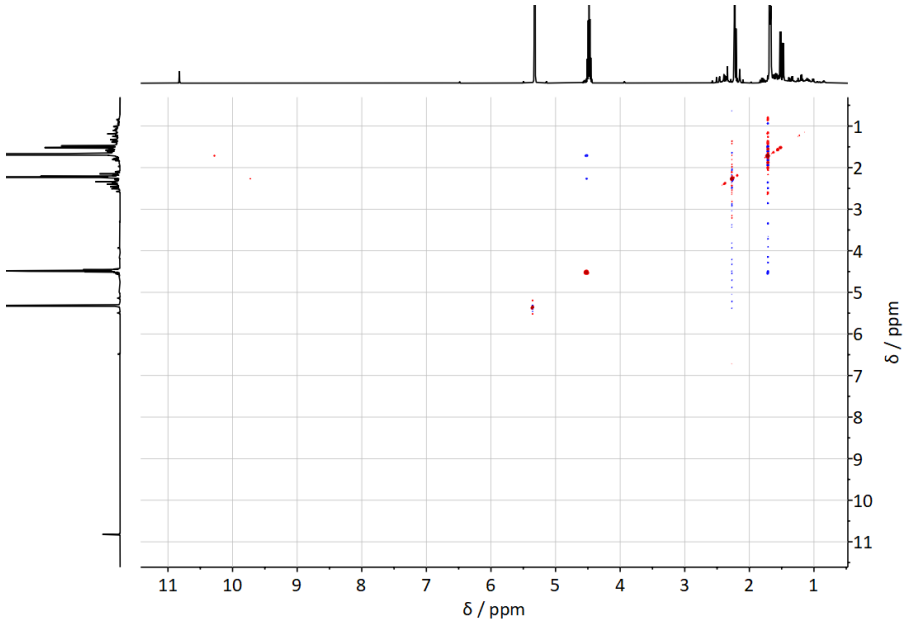

Figure S8: $^{1}H^{1}H$ EXSY NMR spectrum of [iPrH/D]Cl in CD_2Cl_2 at T = 300 K.

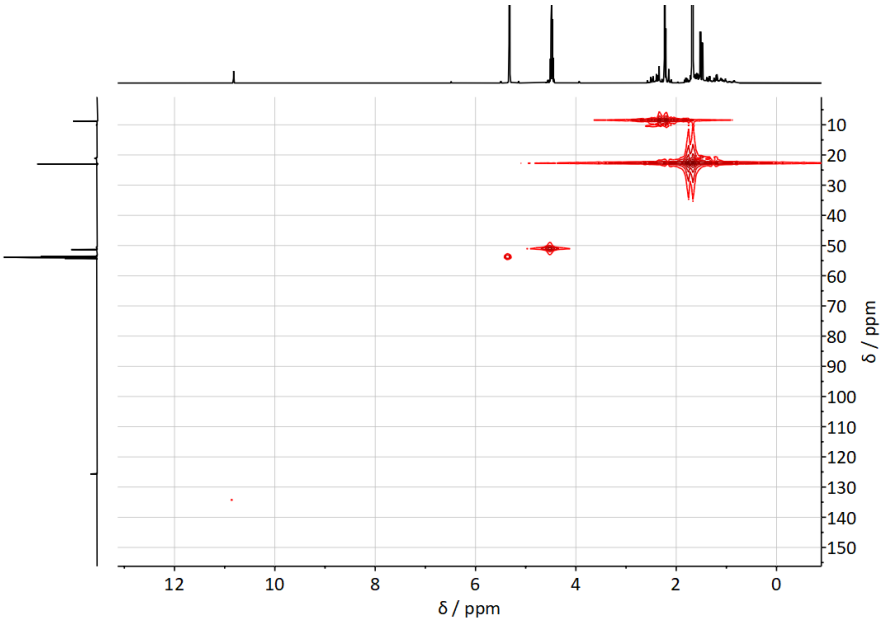

Figure S9: $^{1}H^{13}C$ HMQC NMR spectrum of [iPrH/D]Cl in CD_2Cl_2 at T = 300 K.

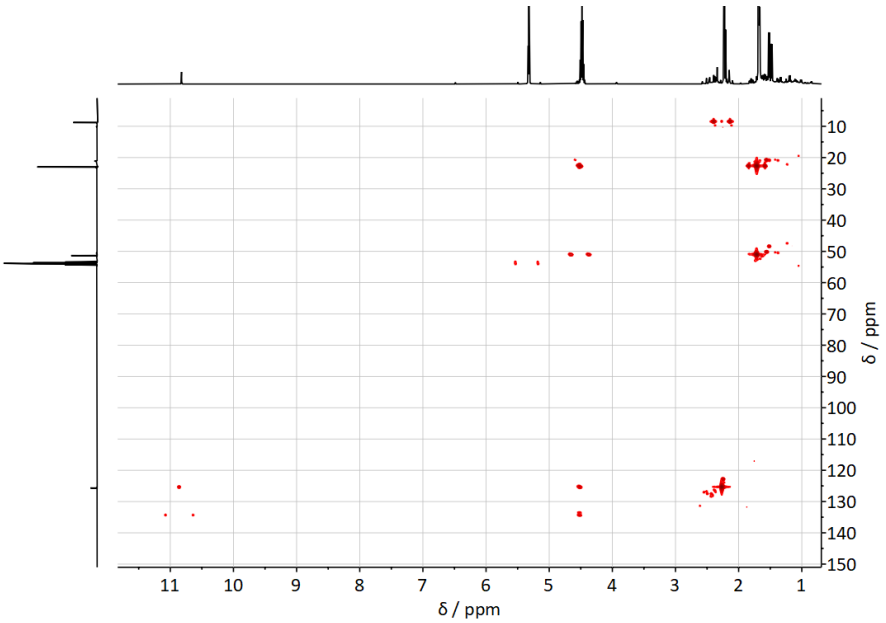

Figure S10: $^{1}H^{13}C$ HMBC NMR spectrum of [iPrH/D]Cl in CD_2Cl_2 at T = 300 K.

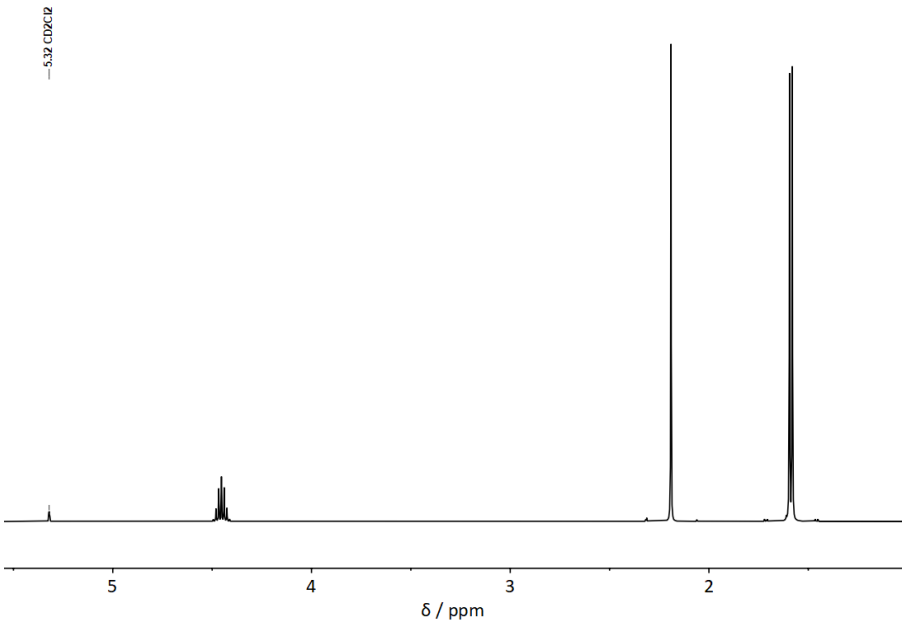

Figure S11: ^{1}H NMR spectrum of [($^{\mathbf{Me}}$**IPr**)$BeBr_2$] in CD_2Cl_2 at T = 300 K.

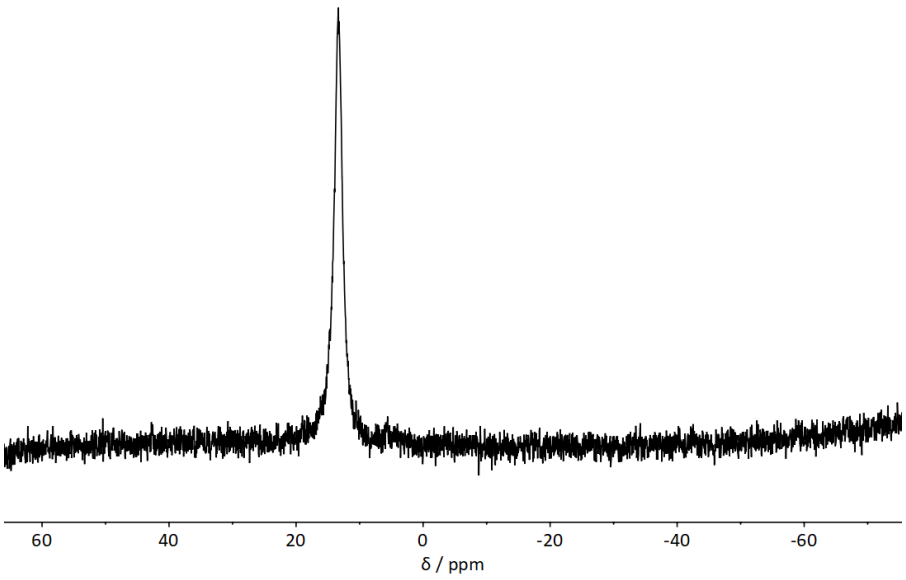

Figure S12: ^{9}Be NMR spectrum of [($^{\mathbf{Me}}$**IPr**)$BeBr_2$] in CD_2Cl_2 at T = 300 K.

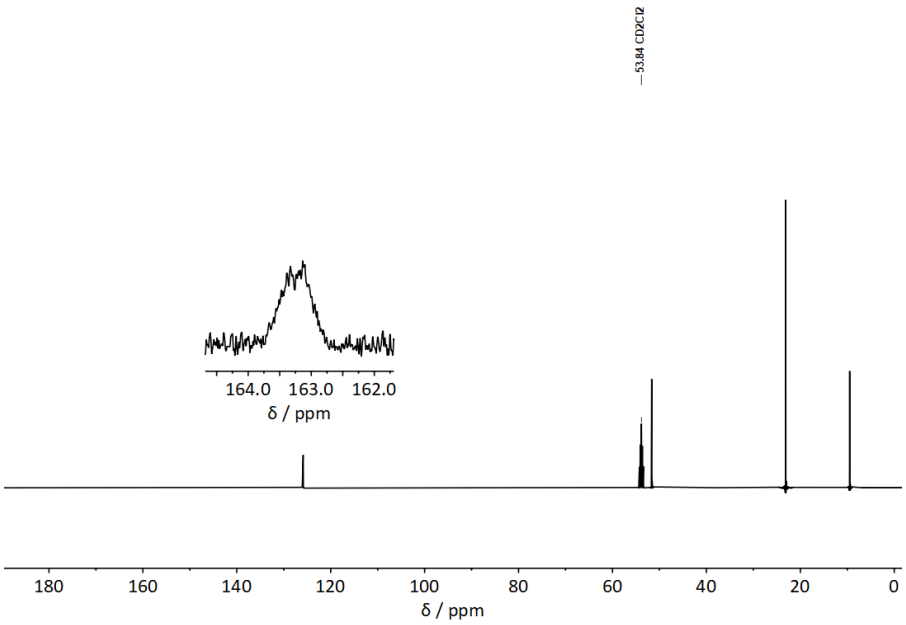

Figure S13: ^{13}C NMR spectrum of [($^{\mathbf{Me}}$**IPr**)$BeBr_2$] in CD_2Cl_2 at T = 300 K.

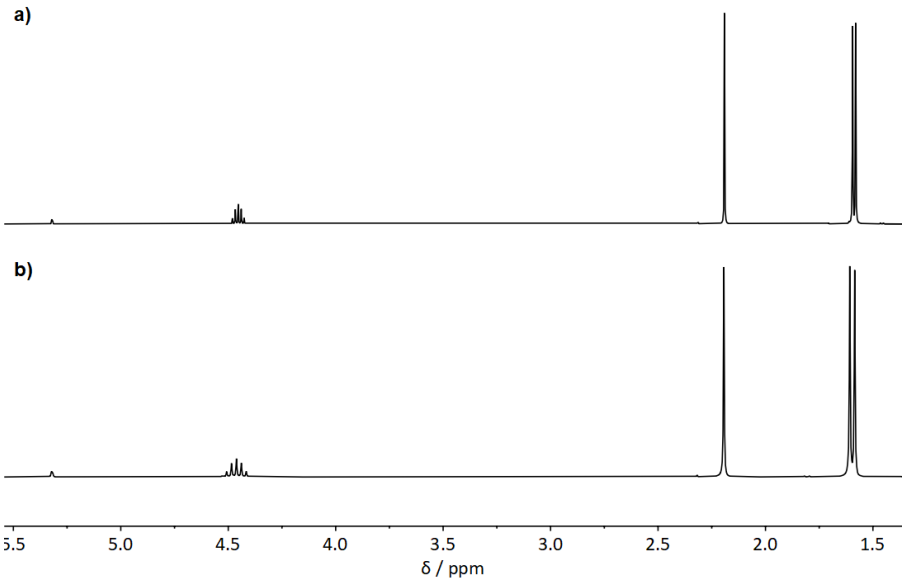

Figure S14: ^{1}H NMR spectra of [($^{\mathbf{Me}}$**IPr**)$BeBr_2$] in CD_2Cl_2, synthesised a) in THF-d^8 and b) through direct combination of $^{\mathbf{Me}}$**IPr** and $BeBr_2$ in CD_2Cl_2. Spectra have been recorded at different field strengths: 500 MHz (top) and 300 MHz (bottom).

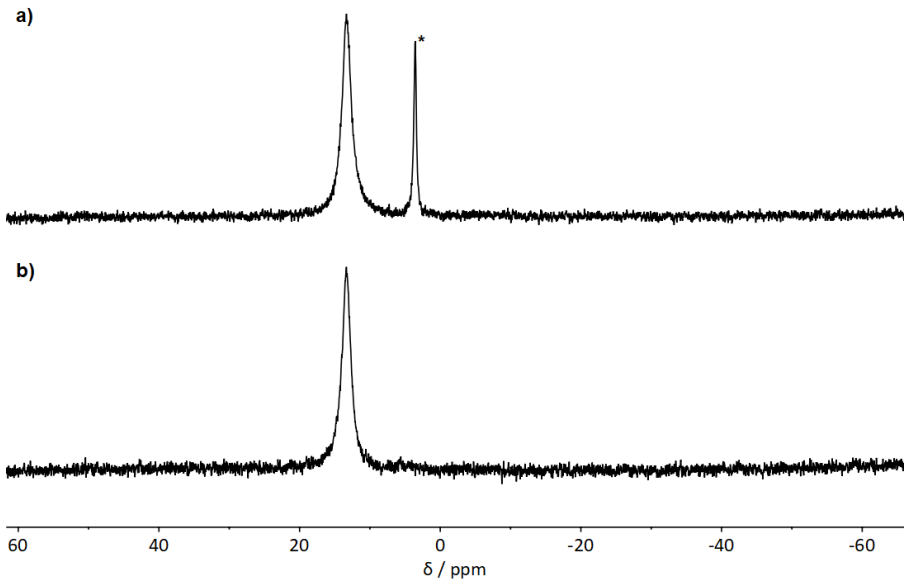

Figure S15: ^{9}Be NMR spectra of [($^{\mathbf{Me}}$**IPr**)$BeBr_2$] in CD_2Cl_2, synthesised a) in THF-d^8 and b) through direct combination of $^{\mathbf{Me}}$**IPr** and $BeBr_2$ in CD_2Cl_2. Some [(THF$-d^8)_2BeBr_2$] from the synthesis is also observable and annotated with an asterisk.

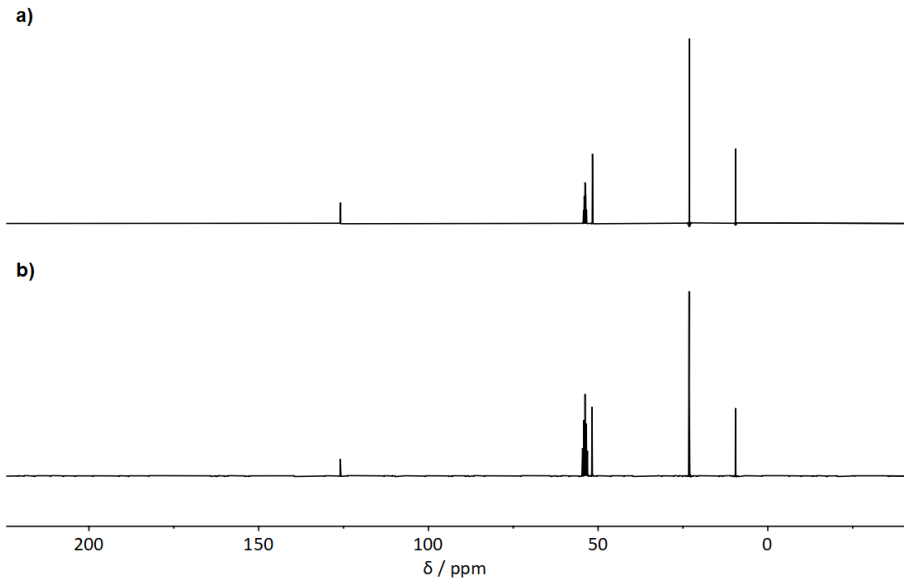

Figure S16: ^{13}C NMR spectra of [($^{\mathbf{Me}}$**IPr**)$BeBr_2$] in CD_2Cl_2, synthesised a) in THF-d^8 and b) through direct combination of $^{\mathbf{Me}}$**IPr** and $BeBr_2$ in CD_2Cl_2.

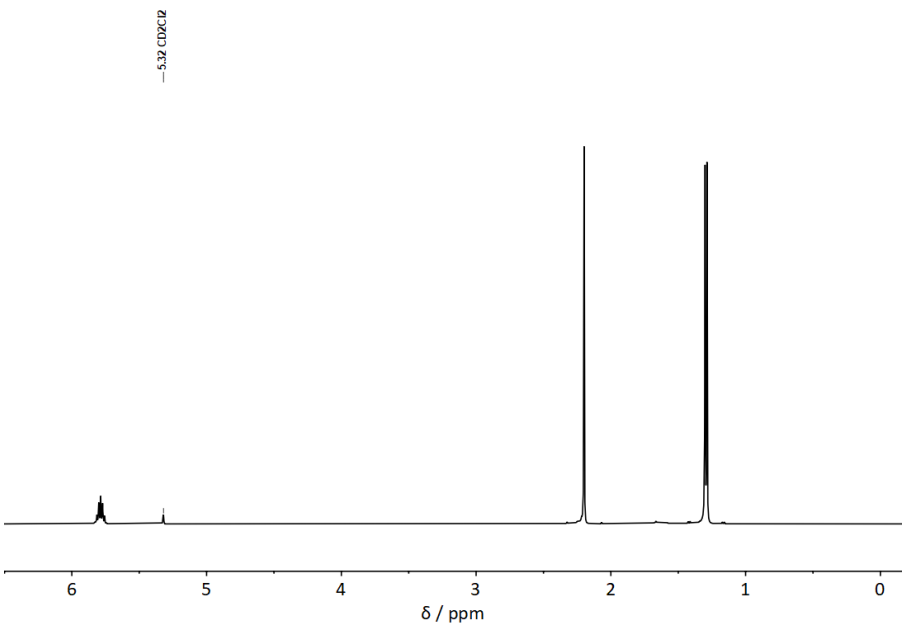

Figure S17: ^{1}H NMR spectrum of [($^{\mathbf{Me}}$**IPr**)$_2$BeBr$_2$] in CD_2Cl_2 at T = 300 K.

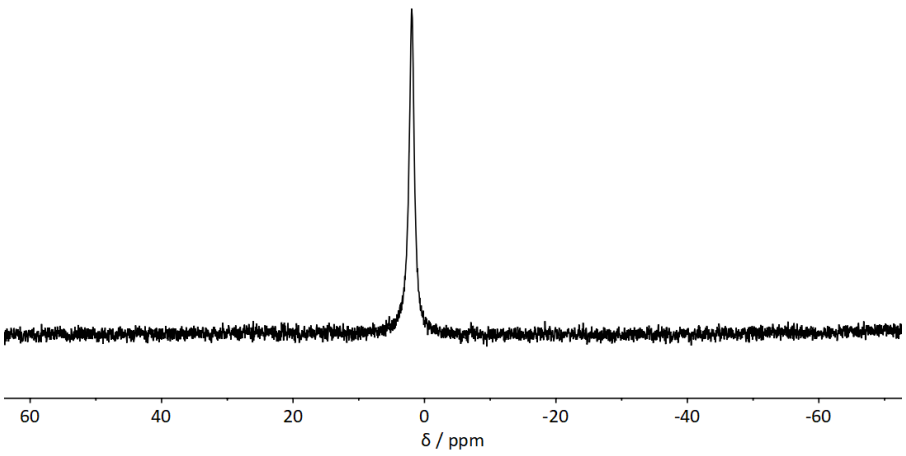

Figure S18: ^{9}Be NMR spectrum of [($^{\mathbf{Me}}$**IPr**)$_2$BeBr$_2$] in CD_2Cl_2 at T = 300 K.

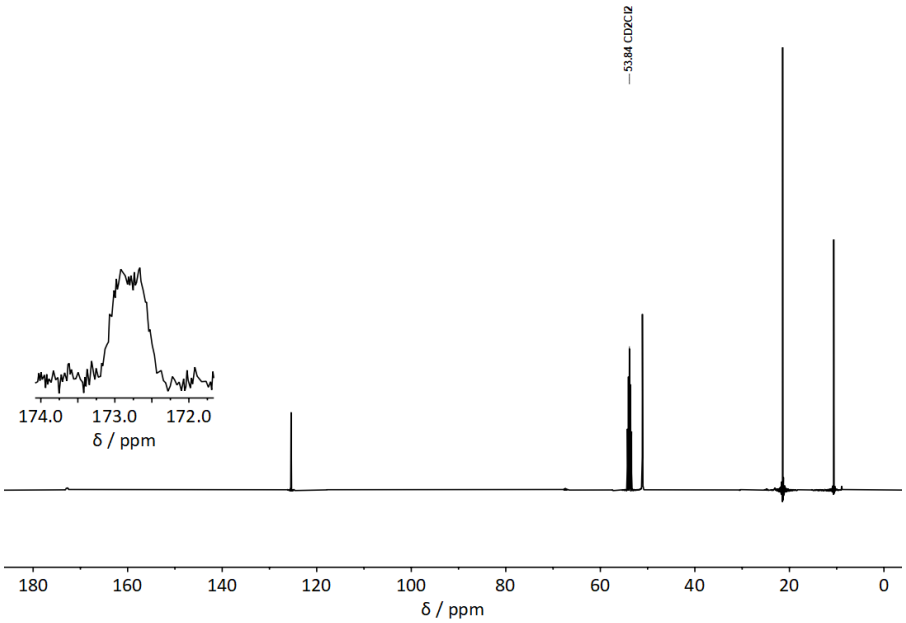

Figure S19: ^{13}C NMR spectrum of [($^{\mathbf{Me}}$**IPr**)$_2$BeBr$_2$] in CD_2Cl_2 at T = 300 K.

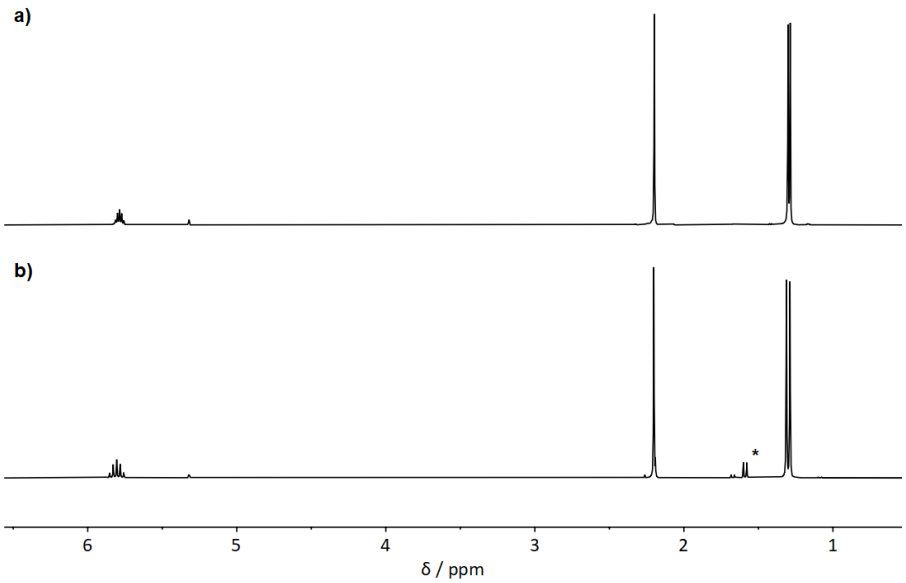

Figure S20: ^{1}H NMR spectra of [($^{\mathbf{Me}}$**IPr**)$_2$BeBr$_2$] in CD_2Cl_2, synthesised a) in THF-d^8 and b) through direct combination of $^{\mathbf{Me}}$**IPr** and $BeBr_2$ in CD_2Cl_2. Traces of [($^{\mathbf{Me}}$**IPr**)BeBr$_2$] is also observable and annotated with an asterisk. Spectra have been recorded at different field strengths: 500 MHz (top) and 300 MHz (bottom).

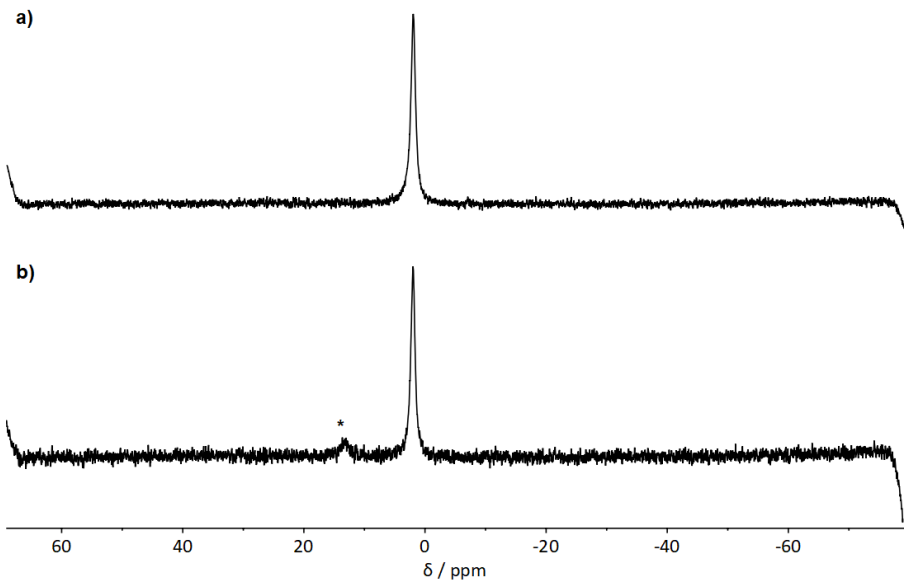

Figure S21: ^{9}Be NMR spectra of [($^{\mathbf{Me}}$**IPr**)$_2$BeBr$_2$] in CD_2Cl_2, synthesised a) in THF-d^8 and b) through direct combination of $^{\mathbf{Me}}$**IPr** and $BeBr_2$ in CD_2Cl_2. Traces of [($^{\mathbf{Me}}$**IPr**)$BeBr_2$] is also observable and annotated with an asterisk.

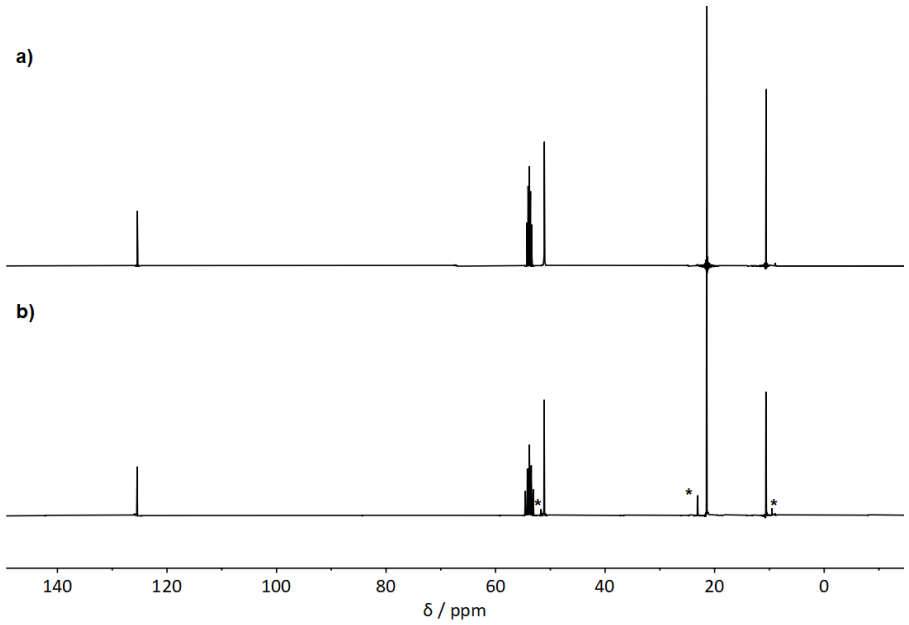

Figure S22: ^{13}C NMR spectra of [($^{\mathbf{Me}}$**IPr**)$_2$BeBr$_2$] in CD_2Cl_2, synthesised a) in THF-d^8 and b) through direct combination of $^{\mathbf{Me}}$**IPr** and $BeBr_2$ in CD_2Cl_2. Traces of [($^{\mathbf{Me}}$**IPr**)$BeBr_2$] is also observable and annotated with an asterisk.

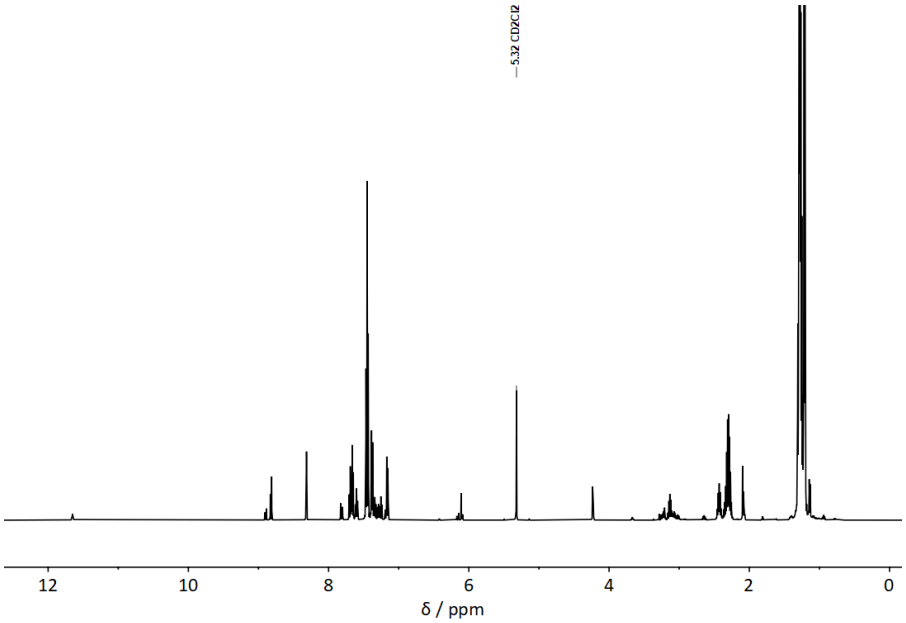

Figure S23: ^{1}H NMR spectrum of **IDipp** in CD_2Cl_2 after 24 h at T = 300 K.

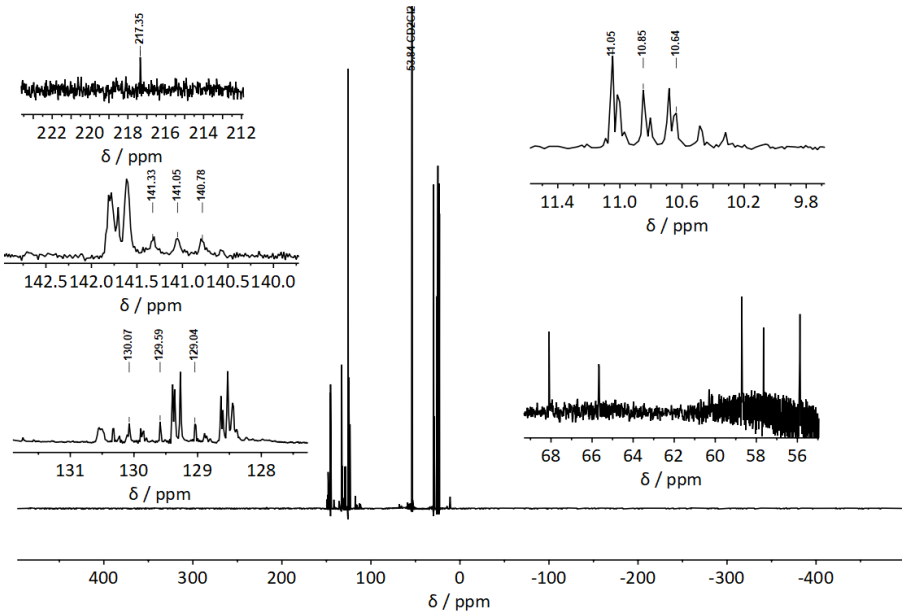

Figure S24: ^{13}C NMR spectrum of **IDipp** in CD_2Cl_2 after 24 h at T = 300 K.

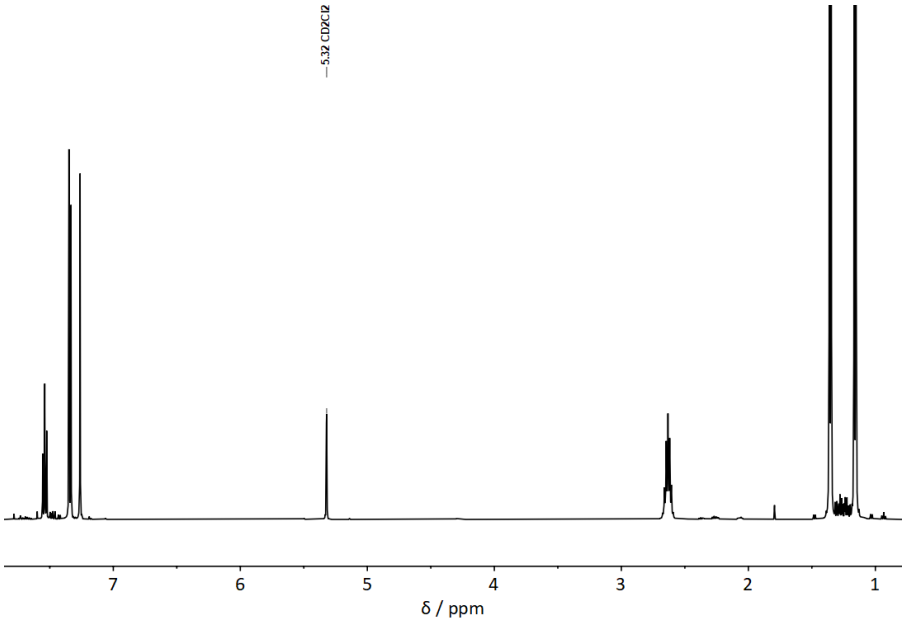

Figure S25: ^{1}H NMR spectrum of [(**IDipp**)$BeBr_2$] in CD_2Cl_2 at T = 300 K.

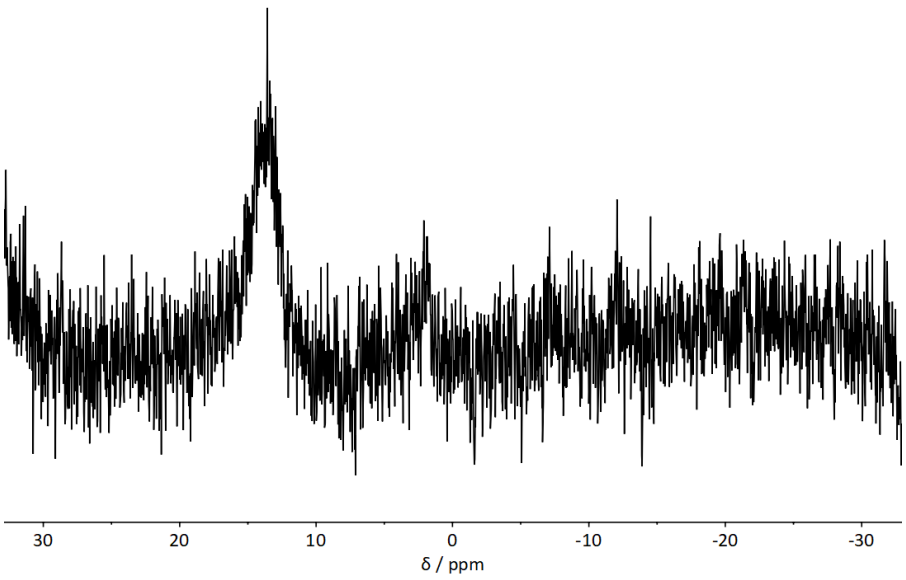

Figure S26: ^{9}Be NMR spectrum of [(**IDipp**)$BeBr_2$] in CD_2Cl_2 at T = 300 K.

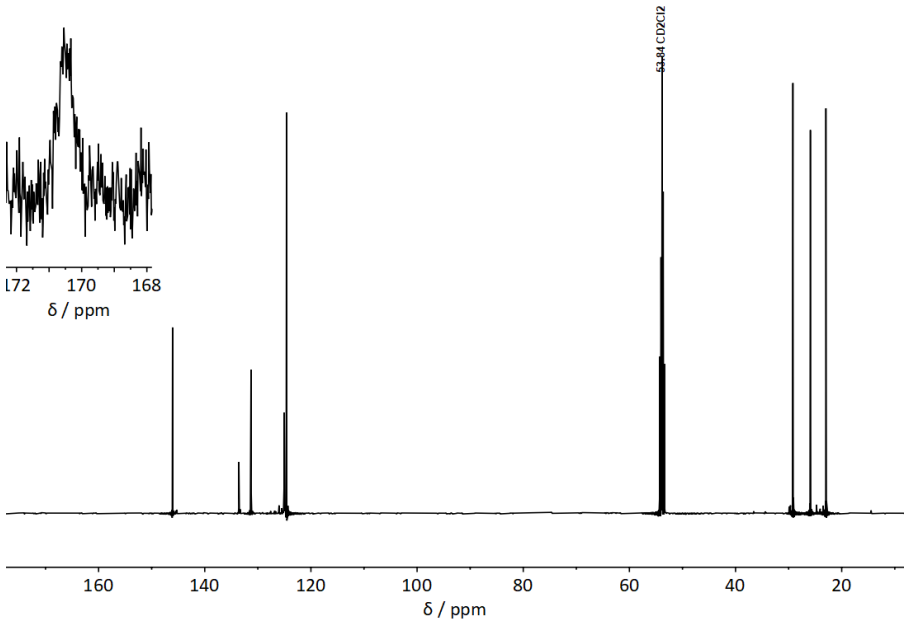

Figure S27: ^{13}C NMR spectrum of [(**IDipp**)$BeBr_2$] in CD_2Cl_2 at T = 300 K.

4 Mass spectrometric data

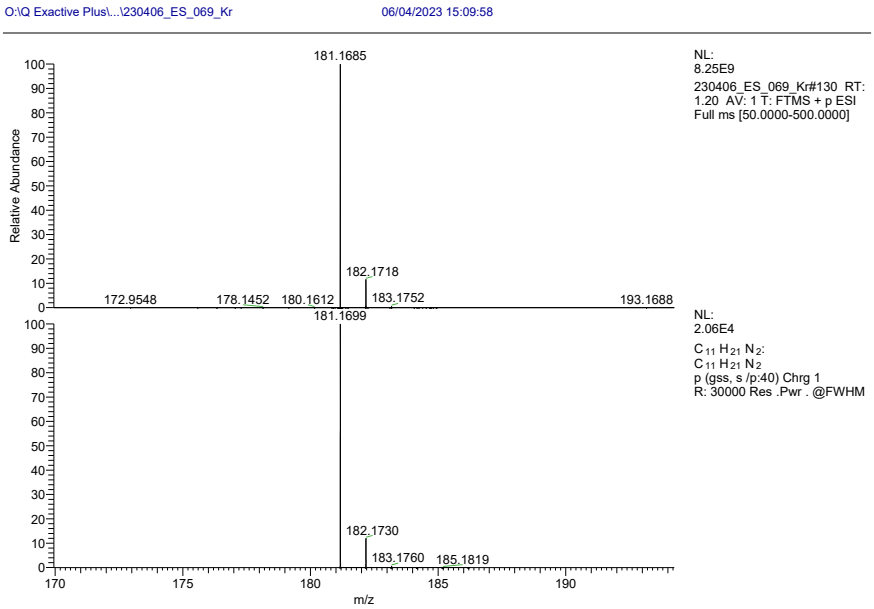

Figure S28: Positive-ion ESI experimental (top) *versus* calculated (bottom) mass spectra of $[^{\mathbf{Me}}\mathbf{IPr}\mathrm{H}]^+$ in CD_2Cl_2 solution.

Table S2: Calculated masses were calculated with the *Isotope Distibution Calculator* with the calculation method *High Resolution*, a minimum abundance of *0.01 %* and an assumed neutral charge. Protonated species completely in DCM. Deuterated species detected in a mixture of H:D (22:100)

calc. (m/z - rel. Intensity)	exp. H (m/z - rel. Intensity)	exp. D (m/z - rel. Intensity)
181.17048 - 100 %	181.1687 - 100 %	–
182.17384 - 11.90 %	182.1721 - 12.09 %	–
182.17675 - 100 %	–	182.1754 - 100 %
183.18011 - 11.90 %	–	183.1787 - 11.40 %

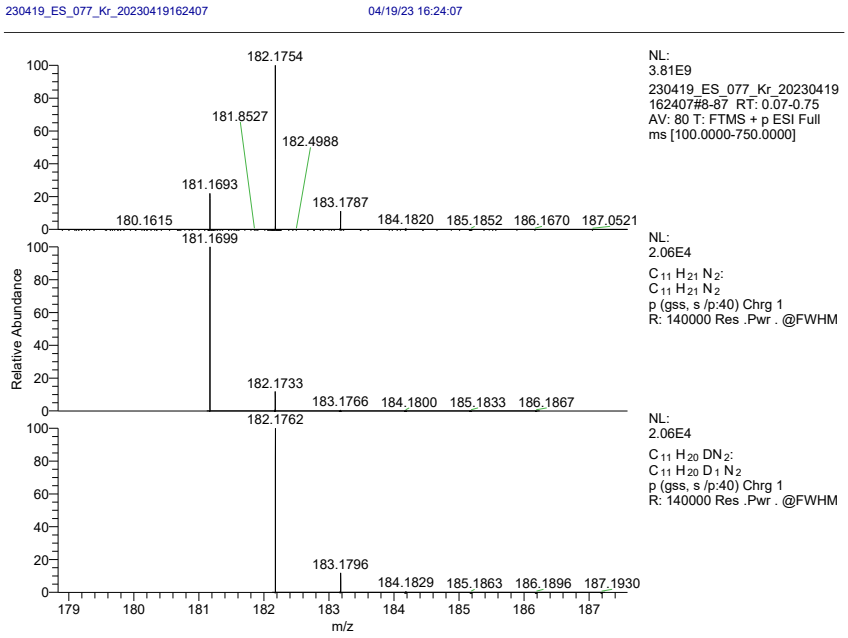

Figure S29: Positive-ion ESI experimental (top) *versus* calculated mass spectra of a mixture of $[^{\mathbf{Me}}\mathbf{IPr}\mathrm{H}]^+$ (middle) and $[^{\mathbf{Me}}\mathbf{IPr}\mathrm{D}]^+$ (bottom) in CD_2Cl_2 solution.

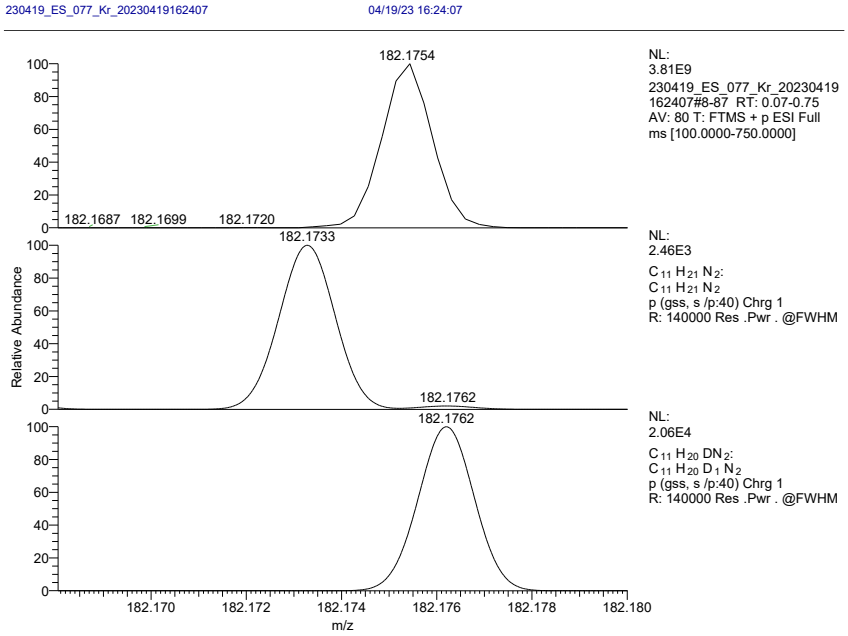

Figure S30: Enlarged sections and normalised positive-ion ESI experimental (top) *versus* calculated mass spectra of a mixture of $[^{\mathbf{Me}}\mathbf{IPr}\mathrm{H}]^+$ (middle) and $[^{\mathbf{Me}}\mathbf{IPr}\mathrm{D}]^+$ (bottom) in CD_2Cl_2 solution.

5 Vibrational spectroscopic data

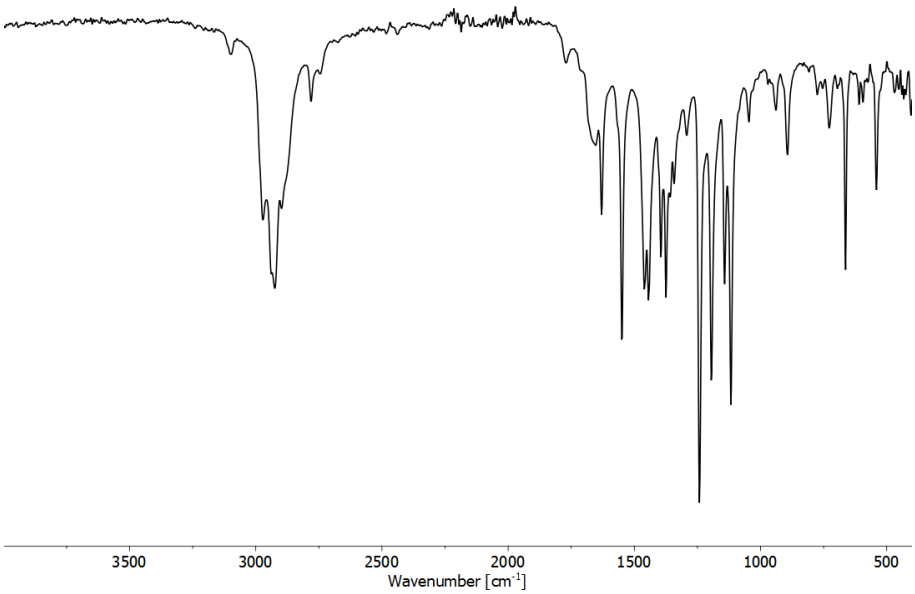

Figure S31: IR spectrum of [$^{\mathbf{Me}}$**IPr**H]Cl.

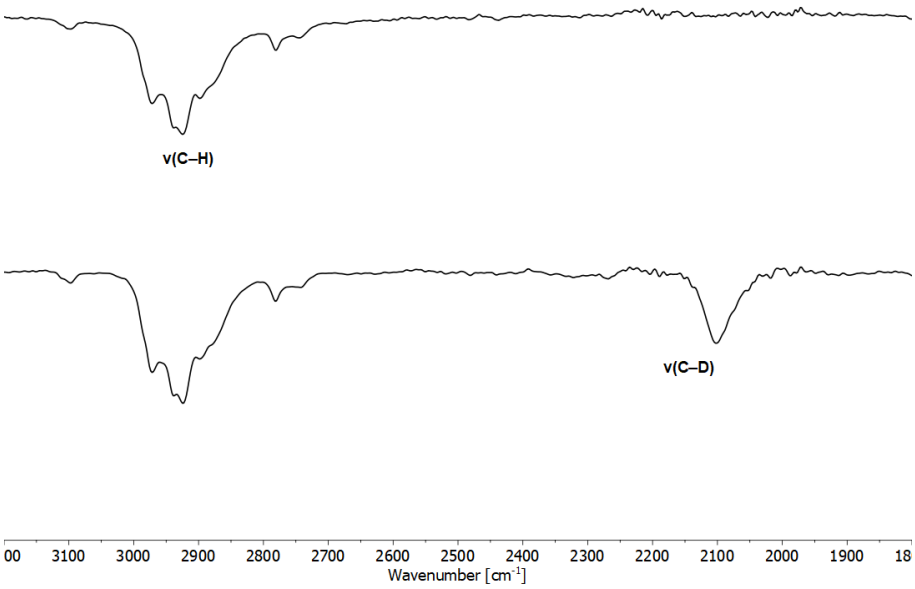

Figure S32: Detail of the IR spectra of [$^{\mathbf{Me}}$**IPr**H]Cl (top) and [$^{\mathbf{Me}}$**IPr**D]Cl (bottom).

6 Kinetic measurements

Inside a glovebox 9.0 mg (0.05 mmol) ^{Me}**IPr** was weighed into a *J. Young* NMR tube and 0.5 ml CH_2Cl_2 was added *via* syringe. After defined time increments (t_1, table S3) the solvent was removed *in vacuo* and the red residue redissolved in CD_2Cl_2. The solutions were left at ambient temperature for defined reaction times (t_2, table S3) to assure complete conversion to [^{Me}**IPr**H/D]Cl before the grade H/D ratio was determined *via* ^{1}H NMR spectroscopy. Please note that the time necessary to remove the solvent *in vacuo* is not accounted for, which results in inaccurate reaction times.

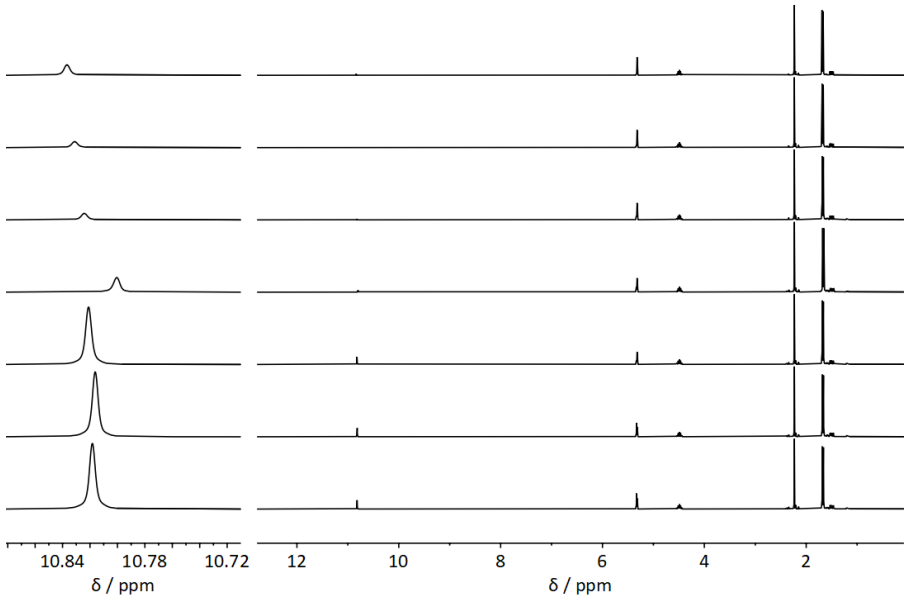

Figure S33: Detail (left) and full ^{1}H NMR spectra (right) of the reaction of ^{Me}**IPr** with CH_2Cl_2 in CD_2Cl_2. Reaction times in CH_2Cl_2 from top to bottom: 0.5 h, 1 h, 2 h, 3 h, 4 h, 5 h and 6 h.

Table S3: H/D ratio dependent on the reaction time of ^{Me}**IPr** in CH_2Cl_2 (t_1) and subsequently in CD_2Cl_2 (t_2) .

t_1 / h	t_2 / h	H/D ratio (NMR) / %
0.5	47.5	0.85
1	47	0.91
2	46	0.90
3	45	0.21
4	44	0.17
5	43	0.05
6	42	0.01

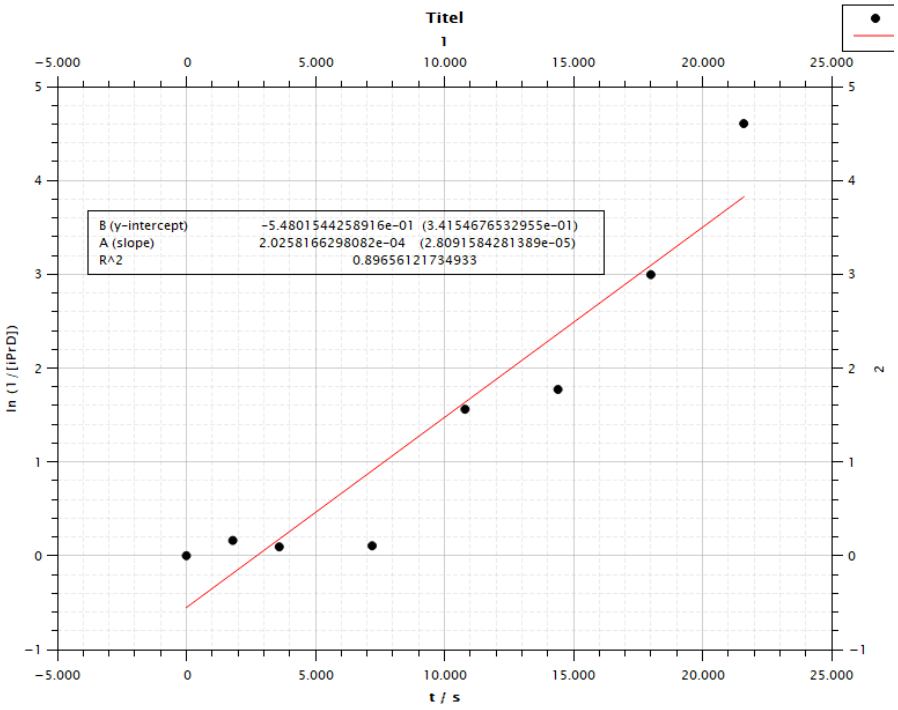

Figure S34: First order fit of the deuteration rates in $[^{\mathbf{Me}}\mathbf{IPr}\mathrm{H/D}]^+$.

7 Notes and references

[1] M. R. Buchner and M. Müller, *ACS Chem. Health Saf.*, 2023, **30**, 36–43.

[2] M. R. Buchner, *Chem. Commun.*, 2020, **56**, 8895–8907.

[3] M. R. Buchner, *Z. Naturforsch., B: J. Chem. Sci.*, 2020, **75**, 405–412.

[4] J. Elguero and I. Alkorta, *Struct. Chem.*, 2023, **34**, 391–398.

[5] D. Naglav, M. R. Buchner, G. Bendt, F. Kraus and S. Schulz, *Angew. Chem. Int. Ed.*, 2016, **55**, 10562–10576.

[6] N. Kuhn and T. Kratz, *Synthesis*, 1993, **1993**, 561–562.

[7] X. Bantreil and S. P. Nolan, *Nat. Protoc.*, 2011, **6**, 69 – 77.

[8] A. Paparo, A. J. R. Matthews, C. D. Smith, A. J. Edwards, K. Yuvaraj and C. Jones, *Dalton Trans.*, 2021, **50**, 7604–7609.

[9] M. Müller, F. Pielnhofer and M. R. Buchner, *Dalton Trans.*, 2018, **47**, 12506–12510.

[10] L. R. Thomas-Hargreaves, S. Pan, S. I. Ivlev, G. Frenking and M. R. Buchner, *Inorg. Chem.*, 2022, **61**, 700–705.

[11] *X-Area 1.8.1*, STOE & Cie GmbH, Darmstadt, Germany, 2018.

[12] G. M. Sheldrick, *Acta Crystallogr.*, 2015, **C71**, 3–8.

[13] G. M. Sheldrick, *Acta Crystallogr.*, 2015, **A71**, 3–8.

[14] O. V. Dolomanov, L. J. Bourhis, R. J. Gildea, J. A. K. Howard and H. Puschmann, *J. Appl. Crystallogr.*, 2009, **42**, 339–341.

[15] K. Brandenburg and H. Putz, *Diamond - Crystal and Molecular Structure Visualization, V 4.6.8*, Crystal Impact GbR, Bonn, 2022.

[16] *MESTRENOVA 14.2.1*, Mestrelab Research S.L., Santiago de Compostela, Spain, 2021.

[17] *OPUS V7.2*, Bruker Optik GmbH, Ettlingen, Germany, 2012.